Brazilian Journal
of Chemical
Engineering

ISSN 0104-6632
Printed in Brazil
www.abeq.org.br/bjche

Vol. 31, No. 02, pp. 503 - 518, April - June, 2014
dx.doi.org/10.1590/0104-6632.20140312s00002521

FOULING BEHAVIOR AND PERFORMANCE OF MICROFILTRATION MEMBRANES FOR WHEY TREATMENT IN STEADY AND UNSTEADY-STATE CONDITIONS

H. Rezaei[1], F. Zokaee Ashtiani[2*] and A. Fouladitajar[2]

[1]Department of Chemical and Biological Engineering, University of British Columbia, Vancouver, Canada.
[2]Department of Chemical Engineering, Amirkabir University of Technology, No. 424, Hafez Ave., Tehran, Iran.
Phone: + 98 21 6454 3124.
E-mail: Zokaee@aut.ac.ir

(Submitted: January 31, 2013 ; Revised: July 31, 2013 ; Accepted: July 31, 2013)

Abstract - Whey pretreatment for protein purification is one of the main applications of cross-flow microfiltration before an ultrafiltration process. In this paper, the effects of the operating pressure and cross-flow velocity on the membrane performance and the individual resistances in microfiltration of whey for both unsteady and steady-state conditions were investigated for two 0.45 μm mean pore size polymeric membranes, Polyethersulfone (PES) and Polyvinylidene fluoride (PVDF). A laboratory-scale microfiltration setup with a flat rectangular module was used. The Reynolds number and operating pressure showed positive and negative effects on the amount of all resistances, respectively. The dominant effect of the concentration polarization and cake resistances was demonstrated by using a "Resistance-in-Series" model for unsteady-state investigations, which could vary during the filtration time. An empirical model revealed a linear relationship between the Reynolds number and permeate flux and a second-order polynomial relationship between the transmembrane pressure and the permeate flux. This empirical correlation, implemented for the limited range of MF operating parameters tested in this article for whey protein, was validated with experimental data and showed good agreement between calculated and experimental data.
Keywords: Microfiltration; Whey; Fouling; Resistance; Empirical Correlation; Modeling.

INTRODUCTION

Whey, a by-product of the dairy industry, is produced during cheese production. Proteins recovered from whey have valuable nutritional properties (Espina *et al.*, 2008). The biochemical oxygen demand (BOD) of whey is 32,000–60,000 mg/L, which leads to very severe disposal problems (Cancino *et al.*, 2006). Therefore, it is important and necessary to fractionate and recycle the proteins from whey. One of the most applicable techniques used for this purpose is a membrane process.

Membrane processes are increasingly used in the dairy industry; the fractionation of whey proteins by microfiltration is one significant example (Mercier-Bonin *et al.*, 2004). Membrane processes have been favored since they reduce the use of heat treatment (Vera *et al.*, 2000), which is particularly an advantage for products that are sensitive to high temperature. Furthermore, no chemical additives are needed, and high chemical oxygen demand (COD) removal efficiencies have been achieved (Abbasi *et al.*, 2010) during these processes. The microfiltration separation processes, unlike traditional methods such as

*To whom correspondence should be addressed

acidification and coagulation, do not destroy the proteins' structure in the solution. Besides, the high performance of the cross-flow microfiltration processes make them suitable for industrial-scale separation, purification and clarification processes in the biological, food, dairy, and pharmaceutical industries.

In spite of the broad applications of membrane filtration, the serious flux decline due to membrane fouling presents a major bottleneck for application of this method, particularly for separating colloidal and protein solutions. This flux decline during microfiltration and ultrafiltration of whey has been attributed to the concentration polarization and membrane fouling, including deposition, pore plugging and protein adsorption in the pores of the membrane (Caric *et al.*, 2000). The formation of a deposit layer leads to additional resistance to permeate flow, while the pore clogging changes the effective membrane pore size and its distribution. Even if these materials form only a very thin gel or cake-layer, the high fouling resistance results in an unacceptable filtration rate value. These phenomena influence the membrane performance in a way that the flux declines to a pseudo-steady state that can be one to three orders of magnitude lower than the initial value (Kwon *et al.*, 2000). The fouling sometimes also causes an undesired rejection of the targeted component in selective filtrations such as protein separation (Chuang *et al.*, 2008).

During filtration of proteinaceous solutions (i.e., whey or milk), it has been observed that proteins tend to foul membranes having pore sizes much greater than the size of the constituent protein monomers or dimers. This is attributed to the presence of protein agglomerates that can be three orders of magnitude larger than the monomers (Kelly and Zydney, 1997). Mechanisms of the membrane fouling are complex and they are related to membrane-particle and particle-particle interactions, which in turn depend on the physicochemical condition of the solution (Palacio *et al.*, 2003; Velasco *et al.*, 2003), system hydrodynamics (Saxena *et al.*, 2009), and membrane properties and structure (Martín *et al.*, 2002).

The nature of the forces or interactions causing fouling is also mentioned in the literature (Martín *et al.*, 2002; Cancino-Madariaga *et al.*, 2012). In any case, fouling could be due to chemical binding, hydrophobicity of the membrane, electrostatic attractions etc. The extent to which these forces are present depends on both the particles in the solution and the membrane material. To overcome the flux decline and to make the membrane process more competitive, many recent studies have been done to minimize fouling and/or membrane development (Chuang *et al.*, 2008; Joshi *et al*., 2011; Pollo *et al.*, 2012; Dong *et al.*, 2012; Mirzaie *et al.*, 2012; Pakizeh *et al.*, 2013). Many approaches, including pretreatment of feed suspension, the use of filter aids, physical inserts, Taylor vortices, and pulsating flow, have been studied to improve the performance of the process. All these approaches are in the direction of reducing the flow resistances during operation. In order to improve membrane performance and decrease filtration fouling, a deep knowledge of the quantity and proportion of each resistance during the membrane process plays a vital role.

Numerous studies have been done to predict the sequence of the resistance formation in the membrane filtration of proteinaceous solutions (Zokaee Ashtiani *et al.*, 1999; Ho and Zydney, 2000a; Ho and Zydney, 2002; Palacio *et al.*, 2003; Ansari *et al.*, 2006; Brião and Tavares, 2012). Protein adsorption in the internal structure of the pores has been reported as the most dominant step in fouling phenomena by some researchers (Bowen and Gan, 1991), while others suppose that flux decline results mostly from surface deposition of a cake including protein aggregates (Jim *et al.*, 1992). Many researchers proved that there is a transition in the fouling mechanism. Zokaee *et al*. (Zokaee Ashtiani *et al.*, 1999) reported a shift from the internal blocking to cake formation during a continuous membrane filtration of a biological solution. Ho and Zydney (Ho and Zydney, 2000b) studied the effects of surface morphology and pore structure of membranes on the initial rate of protein aggregate fouling. They also developed a combined pore blockage and cake filtration model for the fouling of protein aggregates during microfiltration (Ho and Zydney, 2000a) which showed good agreement with the experimental data. In previous work (Rezaei *et al.*, 2010), the influence of the operating pressure and liquid cross-flow velocity on the behavior of the resistances in microfiltration of whey was investigated. The governing fouling mechanisms were investigated using linear forms of classic models, as well as two-phase combined fouling models.

In order to understand the fouling phenomenon, carefully considering each resistance change during the filtration and the effects of various parameters will definitely give positive results. Furthermore, knowledge of the sequence of formation of resistances and the unsteady-state behavior of each resistance will provide valuable information during the design and scale-up stages of these types of membrane processes for industrial purposes. In addition, since resistances are the main obstacle in membranous processes, it is vital to have thorough information about the quality and quantity of their role in

filtration operations in order to set up new techniques and achieve better performance and selectivity.

To the best of our knowledge, no comprehensive study has been performed determining each individual resistance for both steady and unsteady-state condition. In this study, the effects of operating conditions, such as the operating pressure and fluid velocity, on each individual resistance in the steady-state cross-flow microfiltration of whey were investigated using two polymeric membranes, Polyethersulfone (PES) and Polyvinylidene fluoride (PVDF). In addition, the changes of these resistances in unsteady-state microfiltration and their effects on the flux decline were investigated. An empirical correlation was developed for the steady-state permeate flux as a function of the operating pressure and Reynolds number based on the experimental results as well.

MATERIALS AND METHODS

Feed

The feed was prepared by dissolving 250 g of whey powder (Kalleh Dairy Co., Iran) in 5 L of distilled water. The powder composition, provided by the manufacturer, is listed in Table 1.

Table 1: Composition of whey powder.

Lactose, wt.%	Fat, wt.%	DM*, wt.%	Humidity, wt.%	Protein, wt.%
61.4	2.5	98.07	1.93	11.5

* Dry Materials

The permeate solution was manually returned to the feed tank each 5 minutes. Because of the low volumetric ratio of permeate (30-100 ml, depending on the operating conditions) to feed, as well the large feed tank (5 L), the change of protein concentration in the feed tank during every 5-minute time interval was assumed to be negligible and the concentration of the whey protein was considered to be almost constant during the experiment. The solution pH was adjusted to 6.8±0.1 and the feed was prepared at ambient temperature (~ 22 °C).

The conductivity for distilled water was 2 μS/m and for the final whey solution was 380000 μS/m, as determined with a BA 380, EDT Instrument. Protein concentration was measured using absorption spectrophotometry at a wavelength of 280 nm (Jasco, V550 UV/VIS Series spectrophotometer).

Membranes

In this study, two polymeric membranes were used: polyethersulfone (PES) and polyvinylidene fluoride (PVDF). The specifications of both membranes are listed in Table 2. The membranes were highly asymmetric and their surface had a much lower porosity than their bulk. Both membranes were hydrophilic. To prevent drying of the membrane and entrapment of air bubbles in the membrane pores, the membranes were kept immersed in distilled water during the different experiments.

Experimental Setup

A laboratory-scale setup was designed to run the experiments. A schematic flow diagram of this experimental setup is shown in Fig. 1. The required constant operating pressure of the feed solution was provided using a variable speed "Rolling" Pump, controlled by an inverter. Two needle valves were installed on the feed and retentate lines to control the solution velocity. Reynolds numbers varying from 750 to 2500 were achieved by adjusting these valves (which corresponded to 1 to 3.5 L/min feed flows, respectively). A liquid flowmeter (MBLD, UK) was calibrated for the feed in this study and was utilized for the main flow measurement and velocity. Permeate flow rate was measured by timed collection using a digital balance (Sartorius Model GE2120, Edgewood, NY) with an accuracy of 0.01 g. Two pressure gauges were placed directly before and after the membrane holder in order to calculate the trans-membrane pressure (TMP), which varied from 0.5 to 2 bar for different experiments.

One point about the experimental system and design is that the system was not able to reach a Reynolds number of 2500 at a TMP of 0.5 bar (highest Re at lowest TMP). So, the operating pressure was chosen as 1 bar, considering the whole range of Reynolds numbers and minimum possible TMP for ease of control and membrane regeneration.

Table 2: Specification of the membranes used in the experiments.

Material	Pore Size (μm)	Porosity, (%)	Thickness (μm)	TMF* mL / (min.cm^2.bar)	Manufacturer
PES	0.45	80	120	60	Membrane Solution
PVDF	0.45	70	125	29	Millipore

* Transmembrane Flow

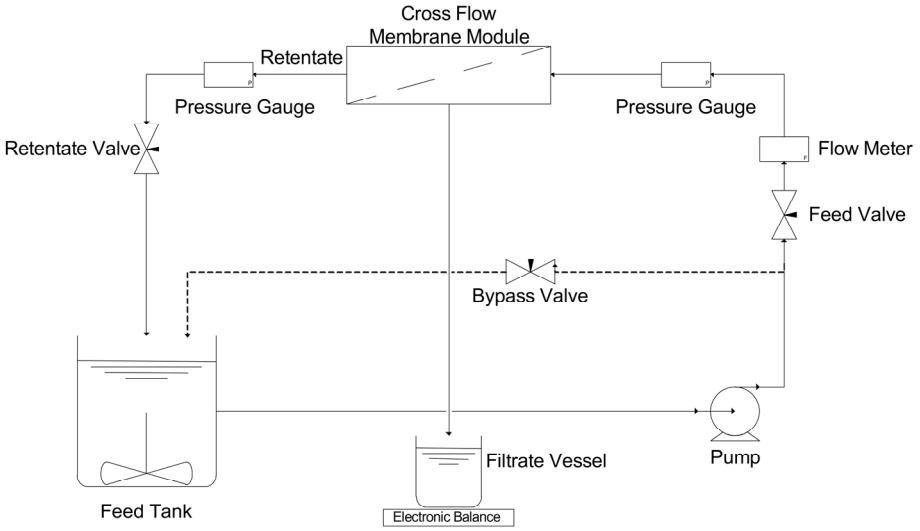

Figure 1: Schematic representation of the laboratory scale microfiltration setup.

The system was able to adjust and control the operating pressure and liquid velocity in the system. Food-grade stainless steel 316 was used for all metallic parts in the experimental setup. The module was made by poly-(methyl-methacrylate) (Perspex), making it possible to observe the phenomena happening inside of the membrane holder (Fig. 2). The membrane holder was in the cross-flow mode. This flat module unit of 215 mm in length and 165 mm in width was used to hold a 10 cm × 5 cm membrane, for a total active membrane area of 0.005 m^2. A very high porosity paper was used as support for the membrane, beneath the membrane, in order to prevent membrane damage at higher pressures; and also make a space for the permeate fluid to move.

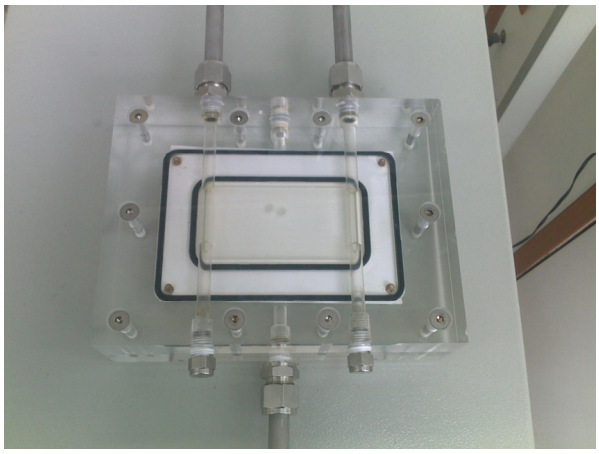

Figure 2: Transparent plexiglass used as the membrane holder in the experiments.

Experimental Procedures

Prior to each protein filtration experiment, the clean water permeate flow was measured in order to determine the degree of membrane cleaning and also the native membrane resistance under each operating condition. Then the feed was circulated in the system under certain operating conditions fixed at the start of each experiment. Furthermore, retentate was recycled to the feed tank and the permeate flux J ($m^3/(m^2.h)$) was determined by timed collection using a digital balance and Eq. (1):

$$J = \frac{1}{A}\frac{dv}{dt} \tag{1}$$

where A is the total active membrane area in m^2, v is the permeate volume in m^3, and t is the filtration time in hours. All the experiments were done in duplicate and results were reproducible with a ±5% error.

The running time per experiment was 40 min. After each filtration step, the unit was emptied, and the solution was collected. Finally, the experimental setup and membrane were rinsed, chemically washed, and cleaned.

The cleaning method was chosen based on the recommendations of the membrane manufacturer and literature (Mohammadi *et al.*, 2003; Madaeni and Mansourpanah, 2004). In all the experiments, a 0.2 wt.% sodium hydroxide (NaOH) solution for 60 min and a 0.2 wt.% nitric acid (HNO_3) solution for

30 min were used for chemical cleaning. The clean water filtration was necessary to identify the regeneration percentage of the membrane at each stage and to determine the state of cleanliness of the membrane for each experiment. In this study, the cleaning method resulted in an almost complete regeneration of the membrane in most of the cases (96-100%). The complete chemical cleaning procedure has been reported in previous work (Rezaei *et al*., 2011). All the chemicals used were supplied by Merck (98 wt.% NaOH, and 67 wt.% HNO3).

In addition, the unsteady-state permeate's protein concentration at an operating pressure of 1 bar and a Reynolds number of 2500 for both PES and PVDF membranes was determined by spectrophotometry at 280 nm. Finally, the results obtained were used to develop an empirical equation for the dependence of permeate flux with TMP and Reynolds number.

Resistance in Series Analysis

The "Resistance-in-Series" model is commonly used to study the role of resistances from different fouling mechanisms. Therefore, the part played by the internal and external fouling in the membranes could be better understood. These resistances include membrane resistance, an external or reversible fouling $R_{rf}(m^{-1})$ which consists of cake layer deposition and concentration polarization, and irreversible resistance, $R_{if}(m^{-1})$. The latter is due to particle and macromolecule deposition and adsorption in the membrane pores.

There are intricate relationships between concentration polarization and cake resistance due to hindered back diffusion within the cake layer. The effects of these two phenomena have been usually considered together; however, some works have taken these two resistances into account separately. The "Resistance-in-series" model and also the method of cake removal described in this work have been used in different works (Matthiasson *et al.*, 1980; Zokaee Ashtiani *et al.*, 1999; Ansari *et al.*, 2006; Brião *et al.*, 2012). Concentration polarization in processes like reverse osmosis (RO) and nanofiltration (NF) may lead to an osmotic pressure which reduces the effective transmembrane pressure. In microfiltration (MF) processes, concentration polarization increases the total resistance and therefore divides the driving force, not subtracting from the TMP.

Accordingly, the total filtration resistance, $R_T(m^{-1})$, can be expressed as Eq. (2):

$$R_T = R_m + R_c + R_{c.p.} + R_{if.} \quad (2)$$

The values of these resistances may be measured experimentally as follows:

- $R_m + R_c + R_{c.p.} + R_{if}$ with the permeate flux measurement at the end of the run;
- $R_m + R_{if} + R_c$ with water flux measurements in situ at the end of the run;
- $R_m + R_{if}$ by water flux measurement after mechanical removal of the deposited cake layer on the membrane surface, gently with a sponge and a 20 minute water flushing;
- R_m by a water flux measurement on a clean membrane.

According to the aforementioned states, the permeate flux was obtained in each step and, using Darcy's law, the resistances were calculated. More details have been given elsewhere (Rezaei *et al.*, 2011).

RESULTS AND DISCUSSION

Resistances in the Unsteady-State Condition

In this study, the values of the unsteady-state fouling resistances were acquired with time for a fixed operating condition at a Reynolds number of 2500 and an operating pressure of 1 bar, for two different polymeric membranes, PES and PVDF. As shown in Fig. 3, the various fouling resistances varied from the early stages of the experiment to long time periods for both membranes. All of them stopped up with increasing time under a definite applied pressure; however, the change in membrane and irreversible resistances was insignificant.

As expected, the membrane resistance for a special and fixed membrane morphology is independent of the fouling and is a function of compaction for polymeric membranes (Rezaei *et al.*, 2010). As a confirmation, the membrane resistance was almost constant for each of the membranes because each membrane material has its own particular morphology. Besides, it is well accepted in the literature (Caric *et al.*, 2000; Martín *et al.*, 2002) that the irreversible fouling depends on the adsorption and the clogging on and/or within the membrane pores. Furthermore, the main irreversible fouling resistance is for the first cycle of membrane use (Mourouzidis-Mourouzis and Karabelas, 2008). Therefore, for studies in which the same membrane has been used for all experiments, the irreversible fouling resistance may be small and also constant among all tests, as indicated in Fig. 3.

The unsteady-state studies were done for two membranes. First, the PES membranes were investigated, which are displayed in Fig. 3(a). The reversi-

ble resistance was the main resistance during all filtration times for this membrane. Thus, it could be demonstrated that the concentration polarization and cake resistances are much more important for the total resistance than other effects. This could also be proved from the percentage of the resistances. During all filtration time periods, the reversible resistance was about 80 percent of the total resistance, while each of the other resistances was less than about 10 percent. Besides, the changing trend of the total resistance was similar to that of the reversible fouling, which proves that the dominance of the reversible fouling resistance. From the beginning of the experiment up to 20th min, increases in the reversible and total resistances were observed, and after that an almost constant value for each of them was achieved. The increase in the resistance value of reversible fouling was due to an increase in the concentration gradient of the protein in the bulk flow on the membrane surface with time, which is because of the pressure-driven convective flow of the solute toward the membrane surface. In turn, this concentration increase created a gel layer, which led to a greater aggregation phenomenon for proteins (Kanani *et al.*, 2008) and then consequently more formation of a cake layer; all of which means increasing reversible fouling. After 20 min, a maximum compaction of the deposited layer and a solute back-diffusion mechanism tended to their maximum value and controlled the membrane permeability. In fact, the convective flow, low porosity cake layer, and back-diffusion of proteins balanced the permeability of the membrane at the final stages of the microfiltration processes, after the 20th minute of operation.

Second, the unsteady-state resistances of the PVDF membrane were investigated and are displayed in Fig. 3(b). The membrane and irreversible resistances were almost constant, or with a negligible variation, as for the PES membrane. The same phenomenon was observed for the unsteady-state filtration with the PVDF membrane. The total resistance had a positive slope for all the range of time periods up to the 20th minute, which confirms the fact that the formation of the deposit layer was continuous during this time, consistent with the work of Tracey and Davis (1994); after 20 min the reversible fouling reached a constant value. The reason of this observation is the same as the previous explanation for the PES membrane.

In addition, the protein concentration in the permeate stream was determined at different times of operation. This protein concentration was based on accumulation.

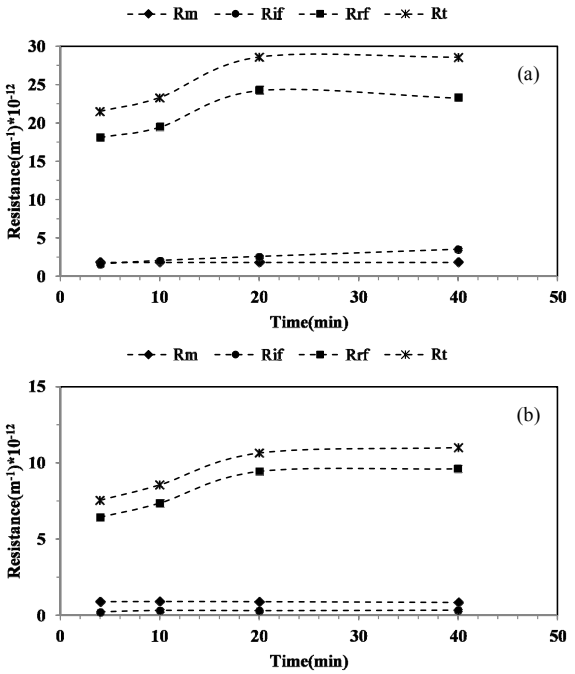

Figure 3: Unsteady-state analysis of the fouling resistances for (a) PES, and (b) PVDF at P=1 bar, Re=2500, and room temperature (22 ± 1 °C).

This means it was different from the exact unsteady-state protein transmission at the times of 4, 10, 20 and 40 minutes. So, it should be taken into account that the protein rejection (%) of the retentate stream was calculated based on accumulated protein concentration in the permeate stream. As shown in Fig. 4, for both PES and PVDF membranes, the permeate's protein concentration increased during the filtration up to the 20th minute, and then reached a constant level. From the beginning of the experiment, the protein concentration increased in the liquid exposed to the membrane surface. This was because of the pressure-driven movement of proteins toward the membrane surface, sequentially increasing the concentration gradient. This could be the reason for the increase in the protein permeability for the first 20 min, before reaching the maximum level of reversible fouling. After this step, the reversible fouling remained constant at its highest value (Tracey and Davis, 1994).

In fact, the cake layer formed acted as a pre-filter, controlling the protein permeability (Ho and Zydney, 1999 and 2000a). Besides, the increasing concentration gradient caused a back diffusion which balanced the protein convection in the direction of the membrane surface, protein permeability, and diffusion to the bulk. Consequently, the amount of protein permeability in Fig. 4 could be described by the amount of reversible fouling resistance, shown in Fig. 3.

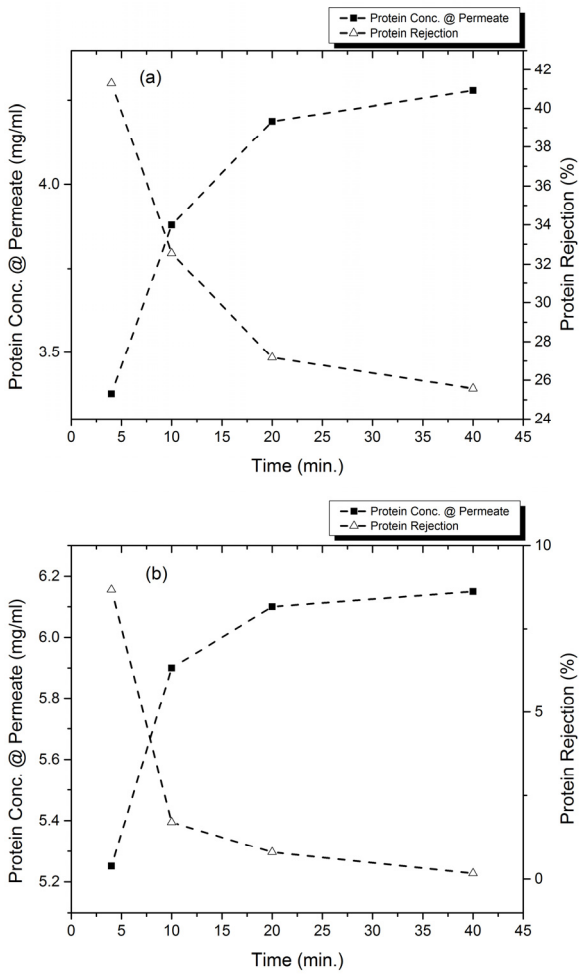

Figure 4: Analysis of the permeate stream protein concentration for (a) PES, and (b) PVDF at P=1 bar, Re=2500, and room temperature (22 ± 1°C).

Resistances in Steady-State Conditions

Membrane Resistance

Fig. 5 shows the experimental data for the membrane resistance and the effect on it of the Reynolds number and the operating pressure, for both the PES and PVDF membranes. The Reynolds number is defined as $\mathrm{Re} = \frac{\rho u D_H}{\mu}$, where D_H (m) is the hydraulic diameter of microfiltration module.

Some tests with deionized water were done and it was observed that the deionized water permeation decreased with time, especially for a new membrane, up to one or two hours when it reached a steady-state condition, as observed by Wang and Tarabara (2008). This membrane compaction was partially reversible between different tests on different days; like the results of Wang and Tarabara (2008), the membrane was pressurized and deionized water circulated for 1 hour before each experiment. This steady-state condition was different for various TMP. The relation between TMP and permeate flux was linear, but did not follow the Darcy Equation. This means that the membrane resistance was changing with TMP. Furthermore, water permeation of the same membrane after a couple of days resting increased a little, indicating that this compression was reversible to some extent. Detailed discussion of the effect of TPM on membrane compaction and the confidential level and dependence of the membrane resistance on Reynolds number and TMP has been explained thoroughly with the statistical method and ANOVA table in previous work (Rezaei *et al.*, 2011). The compaction of the membrane has also been observed is other works (Wang and Tarabara, 2008; Ansari *et al.*, 2006; Zokaee Ashtiani *et al.*, 1999).

The results showed that the membrane resistance varied with the TMP and was independent of Reynolds number. However, there were some small variations in the numbers, about 2%. This negligible difference could have had some other sources, like human error, calculation round off errors, environmental noise factors etc. This result means that the membrane resistance is independent of fouling and the shear due to cross-flow velocity, and is a function of membrane morphology. The resistance dependence on the applied pressure could be described by the compressibility of the polymeric membranes at higher pressures. It was also observed that the majority of this compressibility is reversible during time. The main point in Fig. 5(b) is the similarity of compaction for the two polymeric membranes, especially after the operating pressure of 1 bar in this study. This similarity was observed in unsteady-state behavior from consideration of the resistances in Fig. 3, too.

It can be seen in Fig. 5(b) that the water flux and the resistance were almost equal for the two membranes after 1 bar; and the membrane resistance of PVDF was more than that of PES at an operating pressure of 0.5 bar. This difference at the lowest pressure and the other pressures indicates the clear effect of compaction. Although the initial TMF of the PVDF membrane was about half of this property for the PES membrane (Table 2), it reached the same amount at pressures higher than 1 bar. This phenomenon indicated the severity of the membrane compaction in various ranges of the operating pressure. It was found that the membrane compaction had a dominant influence on the membrane water flux and the resistance.

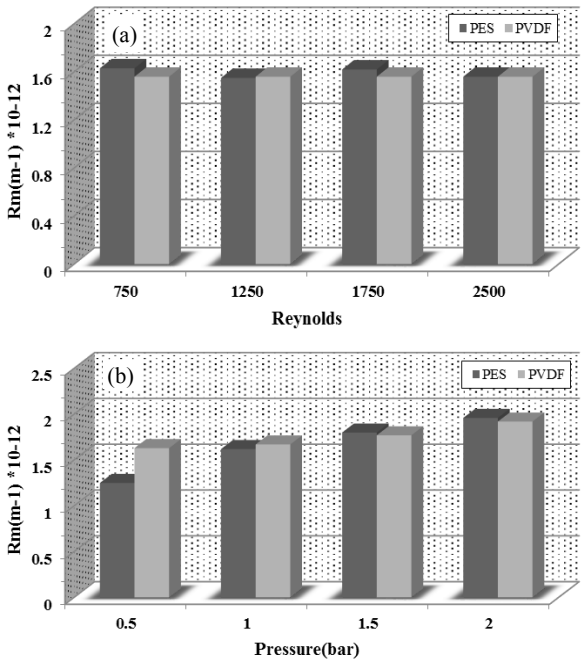

Figure 5: Effect of the operating pressure and Reynolds number on the membrane resistance for the PES and PVDF membranes at (a) P=1 bar, (b) Re=1750, and room temperature (22 ± 1 °C).

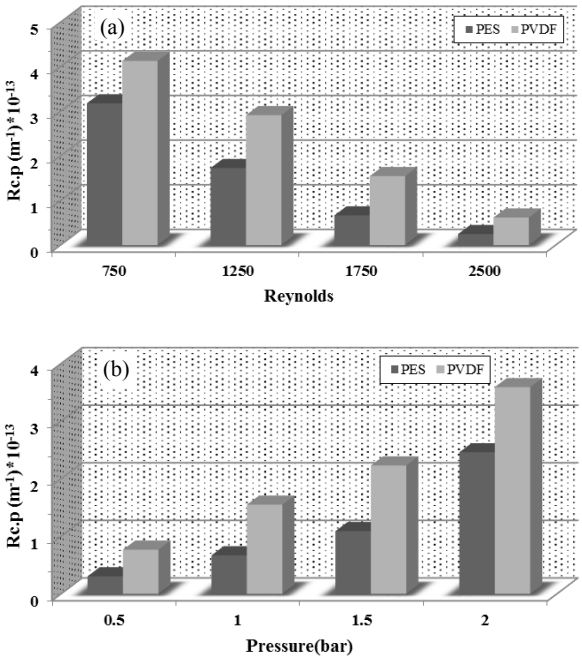

Figure 6: Effect of the operating pressure and Reynolds number on the concentration polarization resistance for the PES and PVDF membranes at (a) P=1 bar, (b) Re=1750, and room temperature (22 ± 1 °C).

Reversible Fouling

Concentration Polarization Resistance

Fig. 6 displays the concentration polarization resistance and its dependence on the Reynolds numbers and the operating pressure, respectively, for both PES and PVDF membranes. As shown in Fig. 6(a), the concentration polarization decreased significantly with increasing Reynolds number. This was due to the fact that the larger the Reynolds number, the higher the shear stress. Accordingly, an increase in shear stress leads to increased mixing, which in turn reduces the thickness of the concentration boundary layer, improving the performance of the membrane. Besides, as observed in Fig. 6(a), reduction of $R_{c.p.}$ took place more effectively and sharply at lower Reynolds numbers, in the laminar region.

In addition, the effect of the operating pressure is obvious in Fig. 6(b). It is clear in the pressure-driven processes that this factor forces the solute molecules toward the membrane surface. So, increasing the applied pressure as a driving force led to more convective transport of the protein molecules to the membrane surface and consequently a larger concentration gradient.

Also, the difference between the amount of concentration polarization resistance of PES and PVDF membranes can be explained based on the "One-dimensional mass transfer model," Eq. (3) (Matthiasson and Sivik, 1980; Gekas and Hallström, 1987):

$$\ln\frac{C_m - C_p}{C_b - C_p} = \frac{J\delta}{D} \tag{3}$$

where C_m is the concentration at the membrane surface, C_p is the permeate concentration, and C_b is the bulk stream concentration. D and δ are the diffusion coefficient and boundary layer thickness, respectively. If the ratio D/δ is defined as the mass transfer coefficient (k), then this equation reduces to Eq. (4):

$$\ln\frac{C_m - C_p}{C_b - C_p} = \frac{J}{k} \tag{4}$$

This is the basic equation for concentration polarization, which depends on two factors, the flux J and the mass transfer coefficient k, and their origin (membrane part, J; and hydrodynamic part, k) re-

sponsible for the concentration polarization. In fact, the mass transfer coefficient, which is a function of system's hydrodynamics, should be constant for the same operating conditions and module flow pattern. Thus, to explain differences between the $R_{c.p.}$ resistances flux results are needed for both membranes; the greater the permeate flux, the larger the concentration gradient.

In order to describe the difference between the $R_{c.p}$, it could be inferred from Eq. (4) that, with increasing permeate flux, the concentration of protein on the membrane surface will increase. Therefore, from this equation and the results of Fig. 9 comparing the fluxes of the two membranes, for the same operating conditions (same k), the concentration near the membrane surface and thus the concentration polarization resistance of the PVDF membrane should be higher than that of PES because of its greater flux (higher *J*).

Cake Resistance

Fig. 7 presents the cake resistance changes versus the Reynolds number and the operating pressure, respectively, for both the PES and PVDF membranes. This observation, as well as concentration polarization, provided an indication of a surface protein layer formation, possibly resulting in more compaction with reduced porosity and/or a thinner layer at increased pressure, which could then lead to a reduced flux.

As displayed in Fig. 6, because of greater convective flow at higher pressures, there should be a larger protein concentration gradient near the membrane surface. In turn, the accumulation of the solutes near the surface boundary layer will increase the possibility of aggregation, consistent with the results of Kanani *et al.* (2008) and Wang *et al.* (2008).

Also, the cake resistance was a function of the Reynolds number; the lift force produced by greater wall shear stress was responsible for preventing the particles from deposition over the membrane length. The same holds for the concentration polarization resistance. This phenomenon can be described by the higher shear stresses resulting from higher velocities. As shown in Figs. 6 and 7, to minimize the concentration polarization and cake resistances, the operating conditions should be at the minimum operating pressure and the maximum cross-flow velocity. In turn, these conditions minimize the role of the main resistance, the reversible fouling resistance, in a filtration process, as mentioned in Fig. 3.

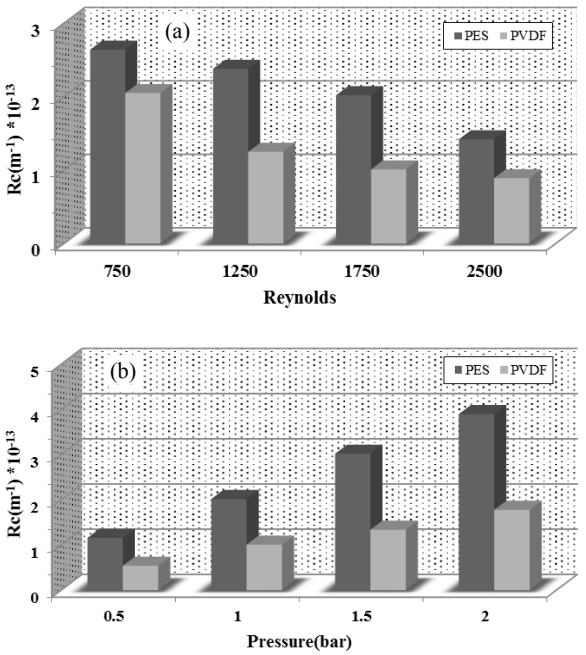

Figure 7: Effect of the operating pressure and Reynolds number on the cake resistance for the PES and PVDF membranes at (a) P=1 bar, (b) Re=1750, and room temperature (22 ± 1 °C).

Irreversible Fouling

Fig. 8 shows the irreversible fouling resistance and its dependency on the Reynolds number and the operating pressure, respectively, for both the PES and PVDF membranes. It is understood (Kanani *et al.*, 2008; Kimura *et al.*, 2008; Mourouzidis-Mourouzis and Karabelas, 2008) that the difference between the initial clean water flux at the beginning of a series of filtration cycles (i.e., before any fouling takes place) and the initial water flux after a backwash, which removes the reversible fouling, represents the flux reduction due to irreversible fouling. This type of fouling was apparently related to the deposition of the particles on and/or within the membrane pores, which will be rarely removed during backwash.

In Fig. 8(a), the effect of Reynolds number on the irreversible resistance proved the positive influence of high cross-flow velocity. In this case, the irreversible resistance was inversely proportional to the Reynolds number. It should be noted that the lift force as a function of the wall shear stress was greater at higher Reynolds numbers. In turn, the cake layer was thinner and the accumulation of material which could increase the irreversible fouling was less. This reduction in material content near the

membrane surface could be because of either cake removal or interruption of the mass boundary layer. Consequently, the likelihood of particle penetration into the pores of the membrane was diminished.

As displayed in Fig. 8(b), the operating pressure had a negative effect on the irreversible resistance and this resistance was proportional to the TMP. This was possibly due to the stronger normal force, which caused the aggregates and the proteins to penetrate into the membrane pores. In addition, as mentioned in the cake resistance section, the use of higher pressures caused an increase in the protein concentration near the membrane surface and, in turn, led to an increase in protein aggregation; so, the effect of the operating pressure was more dominant at its higher values. This fact is displayed clearly in Fig. 8(b) for the PVDF membrane which had a sharper increase after applying a pressure greater than 1 bar.

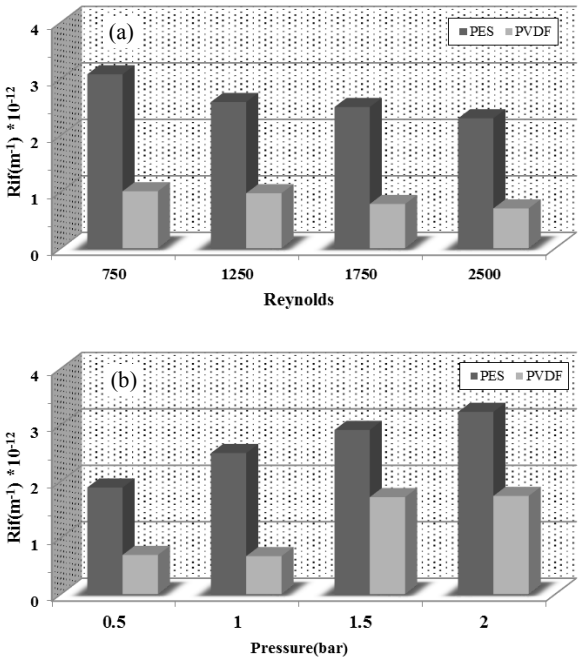

Figure 8: Effect of the operating pressure and Reynolds number on the irreversible fouling resistance for the PES and PVDF membranes at (a) P=1 bar, (b) Re=1750, and room temperature (22 ± 1 °C).

As shown in Fig. 8, the irreversible resistance of the PES membrane was higher than that of PVDF. As known, the irreversible fouling relates to the earlier times of operation (Kanani *et al.*, 2008; Kimura *et al.*, 2008) and could not be described by the steady-state concentration polarization and cake resistances; it is more likely to be explained by the morphology of the membranes. As mentioned previously, the porosity of the PES membrane was 80%, while it was 70% for the PVDF membrane of the same mean pore size. Due to this structure, the probability of particles penetrating into the pores increased. Because of this characteristic, a much wider range of particle sizes could be entrapped in the pores. Besides the TMF, the permeability of PES before any fouling and compaction occurs is twice that of PVDF. This caused more solute convective flow and more permeability in the earlier times of operation, and sequentially more protein adsorption and trapping within the pores. Therefore, the adsorption and clogging of the pores, which are the main reasons of the irreversibility (Caric *et al.*, 2000; Kanani *et al.*, 2008), led to a higher irreversible resistance. Also, it can be seen from Fig. (8) that the effect of pressure is much greater than that of Reynolds number. Like the reversible fouling resistances, the minimum operating pressure and maximum Reynolds number are recommended to minimize the irreversible fouling.

Permeate Flux in Steady- and Unsteady-State Conditions

Effect of Operating Pressure

The steady-state permeate flux versus the operating pressure at a Reynolds number of 1750 is shown in Fig. 9. As displayed in this figure, there is an optimum value for the operating pressure where the steady-state permeate flux is maximum. The optimum operating pressure in this system was found to be 1.5 bar. This means that the filtration performance increased when the operating pressure increased from 0.5 bar to the optimum value of 1.5 bar. For operating pressures lower than 1.5 bar, an increase in operating pressure caused the driving force to increase and this improved the steady state flux. At operating pressures above 1.5 bar, the performance tended to degrade with increased pressure.

This increased operating pressure (greater than 1.5 bar), caused three phenomena to happen: (1) an increase in the driving force, (2) compression of the formed cake and (3) compaction of the membrane. A tendency toward cake formation on the membrane surface appeared when the applied operating pressure increased. This was possibly due to denaturation and aggregation of the proteins induced by compression (Velasco *et al.*, 2003; Kanani *et al.*, 2008). In fact, at high pressures, the intense convective flow of solutes toward the membrane surface and the sharp

concentration gradient in a thinner mass boundary layer are dominant effects. This usually is the reason for forming a cake layer and aggregation of proteins induced by compression, i.e., phenomenon 2. Compaction of the membranes, particularly polymeric membranes, could also be an extra resistance that reduces the permeate flux, as displayed in Fig. 5(b). Therefore, at operating pressures above the optimum condition, the second and third reasons were the dominant phenomena, and compression of the formed cake and compaction of the membrane lead to more severe flux reduction. Based on theoretical considerations, according to the Darcy law, Eq. (5), the effect of the first phenomenon on the TMP; and the second and third ones on the resistance parameter can be seen.

$$J = \frac{TMP}{\mu.R} \tag{5}$$

where J is in $m^3/(m^2.h)$, μ is the permeate viscosity in $(Pa.s)$, and R the resistance in each step in (m^{-1}).

As displayed in Fig. 9, for pressures lower than 1.5 bar, increasing the TMP overcame the increased resistance and resulted in a higher permeate flux. But, at operating pressures above 1.5 bar, the performance tended to degrade with increasing operating pressure. According to Figs. 6(b) and 7(b), the reversible resistances, which were the greater percentage of the resistances, showed a sharper increase after 1.5 bar, and had a more important role in comparison with the TMP for this region. Besides, the compressibility of the membrane for higher pressures, shown in Fig. 5(b), had a negative impact on the permeate flux.

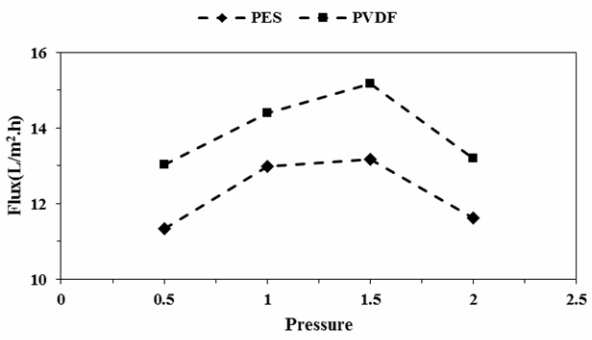

Figure 9: Effect of the operating pressure on the permeate flux for the PES and PVDF membranes in Re=1750, and room temperature (22 ± 1 °C).

In addition, the unsteady-state permeate flux versus time of operation is shown for different applied pressures at a Reynolds number of 1750 in Fig. 10. The flux decline could be classified into two distinct phases in this figure. "Phase I" and "Phase II" in Figure 10 separated the sharp flux reduction in the first 5-10 minutes of the process from the gradual reduction up to the 20th minute and the steady-state condition after that. There was a quite rapid reduction in the earlier times of operation in Phase I, and a slow-rate reduction that continued for the rest of the filtration process. This phenomenon could be explained by the unsteady-state behavior of the resistance in Fig. 3. As shown in Fig. 3, the reversible fouling had an increasing effect during the first 20 min for both membranes, while membrane and irreversible resistances were almost constant. After that, the reversible fouling resistance, the main resistance, reached a pseudo-steady state value. In fact it was a transition condition for the fouling mechanism during the process. It is necessary to mention that the 20th min was just a particular operating condition of this study. This number could be different for other operating conditions; however, it was the same for the two membrane materials. Therefore, the existence of this transition time for all conditions was an important point that was observed.

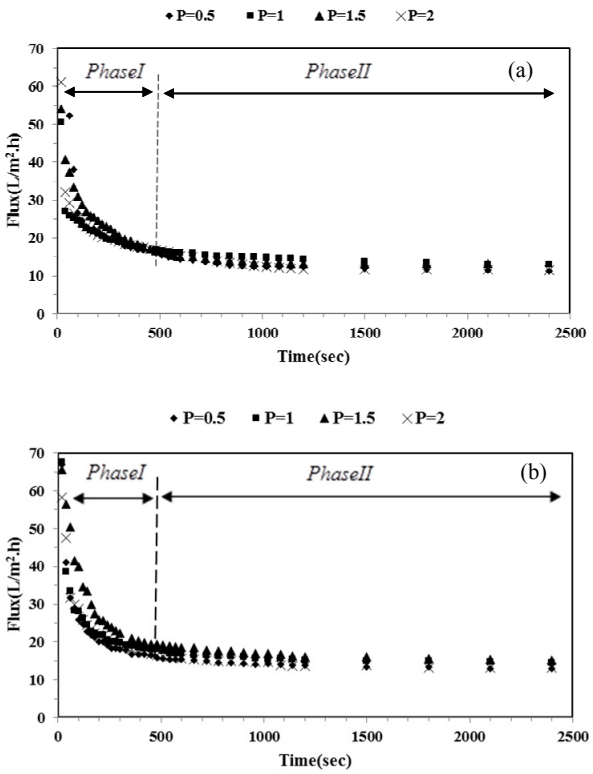

Figure 10: Effect of the operating pressure on flux for (a) PES and (b) PVDF membranes in Re=1750 and room temperature (22 ± 1 °C).

Effect of Cross-Flow Velocity

The final permeate flux versus Reynolds number is shown in Fig. 11. As expected, the limiting permeate flux increased with increasing cross-flow velocity due to higher shear stress.

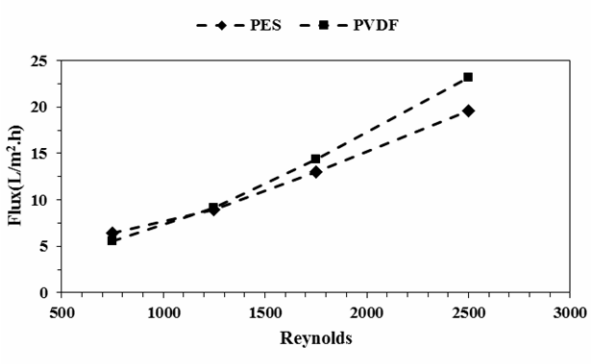

Figure 11: Effect of Reynolds number on the permeate flux for the PES and PVDF membranes at P=1 bar, and room temperature (22 ± 1 °C).

Accordingly, increasing the cross-flow velocity resulted in an increase of the mass transfer coefficient and the concentration gradient layer interruption, shown in Fig. 6(a). Besides, with increasing cross-flow velocity of the liquid feed, the resultant shear stress caused a lift force, preventing the particles to deposit on the membrane surface, Fig. 7(a). The main point derives from comparison of Figs. (9) and (11) is the greater influence of Reynolds number on the steady-state permeate flux than the operating pressure, as proved in previous work (Rezaei *et al.*, 2011).

For the statistical analysis, ANOVA calculations were done for the PES membrane. Table 3 presents the sum of squares (SS), the mean square (variance), and the factor variance to error variance ratio (F), with the level of significance set to 0.05. For the F-values, the greater the value the greater the contribution to the final results. Hence, the results confirmed that a cross-flow velocity increase had a more significant effect on the process efficiency than increasing operating pressure (Table 3). The permeate volume was measured as a function of time until the flux reached an almost constant value. Fig. 12 describes the typical behavior of permeate flux versus time for a certain operating condition (different Re numbers and TMP=1). As displayed, the same reduction trend was observed in all cases and the required time was always less than 2400 s. As depicted in Fig. 12, the higher the Re numbers, the higher the permeate flux. This confirms that higher velocities lead to higher shear forces and, consequently, higher shear stress leads to increased mixing, which in turn reduces the size of the concentration boundary layer and increases the permeate flux.

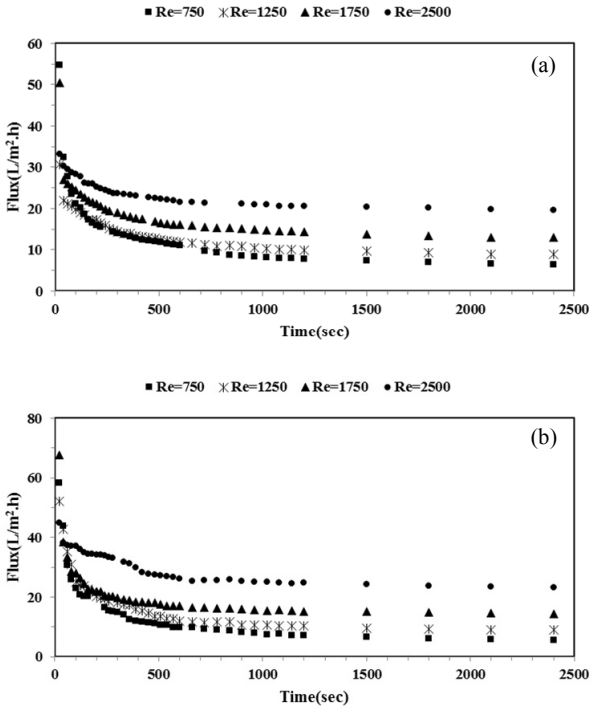

Figure 12: Effect of Reynolds number on flux for (a) PES and (b) PVDF membranes at P=1 bar and room temperature (22 ± 1 °C).

Table 3: ANOVA table for the PES membrane experiments.

Source	DF	Seq. SS	Adj. SS	Adj. MS	F	P
Re	3	749.654	749.654	249.885	25289.43	0.000
Pressure	3	34.069	34.069	11.356	1149.33	0.000
Re*Pressure	9	18.940	18.940	2.104	212.98	0.000
Error	16	0.158	0.158	0.010	-	-
Total	31	802.821	-	-	-	-

Experimental Model for Limiting Permeate Flux

As mentioned earlier, numerous studies have been done to investigate the effect of operating parameters on the performance of membrane processes. Samuelsson *et al*. (1997) proposed an experimental equation to predict the limiting flux in the pseudo-steady state condition for whey microfiltration based on his experimental results. They reported a linear relation between limiting flux and cross-flow velocity for two temperatures, 15 and 55 °C, and a fixed operating pressure of 1 bar. In this study, we extend this equation to express the final flux in terms of Reynolds number and operating pressure. It is important to mention that the validity of this equation is limited to the range of MF operating parameters tested in this article and for whey protein. The pressure and Reynolds number varied from 0.5 to 2 bar and 750 to 2500, respectively.

It was found from the results (Figs. 9 and 11) that there was an almost linear relation between the permeate flux and Reynolds number, with a positive slope, and a non-linear dependence on the applied pressure with a maximum value.

$$Lim.flux = F(P).G(\mathrm{Re}) \quad (6)$$

In fact, at every operating pressure, $F(P)$ was constant and $G(\mathrm{Re}) = \mathrm{Re}$.

$$Lim.flux = F(P).\mathrm{Re} \quad (7)$$

It was found that the flux dependence on the pressure can be best described by Eq. (8), for both the PES and PVDF membranes:

$$Lim.flux = [aP^2 + bP + c].\mathrm{Re} \quad (8)$$

Fitting this equation to the experimental data for both membranes provided the constant coefficient and the results displayed in Table 4.

In addition, the calculated data showed good agreement with the experimental data, presented in Tables 5 and 6. The experimental and calculated fluxes are compared for different operating parameters and the values of the errors are reported for both PES and PVDF membranes.

Table 4: Constant coefficients of the experimental model for both the PES and PVDF membranes.

M.M*	*a*	*b*	*c*	*Average*|%Error|	R^2
PES	-2.194×10^{-3}	5.414×10^{-3}	4.354×10^{-3}	3.83	0.979
PVDF	-2.29×10^{-3}	5.794×10^{-3}	5.118×10^{-3}	6.6	0.944

* Membrane Material

Table 5: Agreement of the experimental model with the experimental data for the PES membrane.

Pressure (bar)	Reynolds	Flux (L/m^2.h)	Cal.* Flux	Residual	%Error
0.5	1750	11.3278	11.4166	-0.0888	-0.7841
1	1750	12.9830	13.3337	-0.3507	-2.7009
1.5	1750	13.1040	13.3704	-0.2664	-2.0333
2	1750	11.6158	11.5269	0.0888	0.7646
1	750	6.4080	5.7144	0.6936	10.8236
1	1250	8.9000	9.5240	-0.6240	-7.0117
1	2500	19.5840	19.0481	0.5359	2.7365

* Calculated

Table 6: Agreement of the experimental model with the experimental data for the PVDF membrane.

Pressure (bar)	Reynolds	Flux (L/m^2.h)	Cal.* Flux	Residual	%Error
0.5	1750	13.0320	13.0255	6.5222×10^{-3}	0.0500
1	1750	14.4000	15.0891	-0.6891	-4.7856
1.5	1750	15.1682	15.1487	0.0196	0.1290
2	1750	13.1976	13.2041	-6.5222×10^{-3}	-0.0494
1	750	5.5678	6.4668	-0.8990	-16.1467
1	1250	9.0950	10.7779	-1.6829	-18.5041
1	2500	23.1358	21.5559	1.5799	6.8287

* Calculated

As displayed in Tables 4 and 5, the percent error in 2 operating conditions, P=1, Re=750 and P=1, Re=1250 was higher than for the others. These are the lower range of Reynolds numbers in the laminar regime of flow, where the fouling mechanisms are maximized. Based on the results, the optimum operating conditions for microfiltration of protein-containing feeds is maximum Reynolds number, the use of this correlation in order to predict the steady-state flux for optimum conditions is suggested.

CONCLUSIONS

The unsteady-state resistances of both PES and PVDF membranes were investigated. It was demonstrated that, for both membranes, the reversible resistance was the dominant resistance, about 80% of the total resistance for the whole filtration time, while each of the other resistances was less than about 10 percent. In the first 20 min of operation, there was a sharp increase in the reversible and the total resistances. After that, an almost constant value was achieved for each of them. This time could be different for other operating conditions; however, there is always a definite time at which this happens.

In considering the unsteady-state permeate flux, there was a quite rapid reduction at the earlier times of operation and a slow-rate reduction for the rest of the filtration. These phenomena were explained by the unsteady-state behavior of the resistances. In addition, the steady-state resistances were also studied. It was found that the dominant resistance reducing the permeate flux is the reversible fouling, including concentration polarization and cake layer formation; the optimum parameters to achieve minimum resistances, especially minimum concentration polarization and cake resistances, were proposed to be minimum applied pressure and maximum Reynolds number. However, this achieves minimum resistances, not energy consumption optimization. Higher feed velocities consume higher energy. The energy and economic analyses should be carried out to investigate the optimum operating parameters.

An empirical correlation was proposed to estimate the limiting flux of cross-flow whey microfiltration as a function of operating pressure and Reynolds number, valid for the range of pressure from 0.5 to 2 bar and Reynolds numbers from 750 to 2500. This correlation was validated with the experimental data and showed good agreement between experimental and calculated data for almost all operating parameters for both PVDF and PES membranes.

NOMENCLATURE

A	Total active membrane area	m^2
C_m	Concentration at the membrane surface	kg/lit
C_b	Concentration in the bulk flow	kg/lit
C_p	Concentration in the permeate flow	kg/lit
D	Diffusion coefficient	$\frac{m^2}{s}$
J	Permeate flux	$\frac{m^3}{m^2.s}$
R^2	Determination coefficient of a linear regression	
Re	Reynolds number	dimensionless
R_m	Membrane resistance	m^{-1}
R_T	Total membrane resistance	m^{-1}
R_c	Cake resistance	m^{-1}
$R_{c.p.}$	Concentration polarization resistance	m^{-1}
R_{rf}	Reversible fouling resistance	m^{-1}
R_{if}	Irreversible fouling resistance	m^{-1}
t	Filtration time	s
TMF	Trans-membrane flow	$ml/min.cm^2.bar$
TMP	Trans-membrane pressure	Pa
V	Collested filtrate volume per unit filtration area	m^3/m^2
v	Permeate volume	m^3

Greek Letters

μ	Permeate viscosity	Pa.sec
δ	Boundary layer thickness	M

REFERENCES

Abbasi, M., Salahi, A., Mirfendereski, M., Mohammadi, T. and Pak, A., Dimensional analysis of permeation flux for microfiltration of oily wastewaters using mullite ceramic membranes. Desalination, 252, 113-119 (2010).

Ansari, S., Zokaee Ashtiani, F., Kaghazchi, T. and Masoodi, S., Study of microfiltration of sweet cheese whey. Afinidad, 63, 303-307 (2006).

Brião, V. B. and Tavares, C. R. G., Pore blocking mechanism for the recovery of milk solids from dairy wastewater by ultrafiltration. Brazilian Journal of Chemical Engineering, 29, 393-407 (2012).

Bowen, W. R. and Gan, Q., Properties of microfiltration membranes: Adsorption of bovine serum albumin at polyvinylidene fluoride membranes. Journal of Colloid and Interface Science, 144, 254-262 (1991).

Cancino-Madariaga, B., Ruby, R., Astudillo Castro, C., Saavedra Torrico, J. and Lutz Riquelme, M., Analysis of the membrane fouling mechanisms involved in clarified grape juice ultrafiltration using statistical tools. Industrial & Engineering Chemistry Research, 51, 4017-4024 (2012).

Cancino, B., Espina, V. and Orellana, C., Whey concentration using microfiltration and ultrafiltration. Desalination, 200, 557-558 (2006).

Caric, M. D., Milanovic, S. D., Krstic, D. M. and Tekic, M. N., Fouling of inorganic membranes by adsorption of whey proteins. Journal of Membrane Science, 165, 83-88 (2000).

Chuang, C.-J., Wu, C.-Y. and Wu, C.-C., Combination of crossflow and electric field for microfiltration of protein/microbial cell suspensions. Desalination, 233, 295-302 (2008).

Dong, C., He, G., Li, H., Zhao, R., Han, Y., Deng, Y., Antifouling enhancement of poly(vinylidene fluoride) microfiltration membrane by adding $Mg(OH)_2$ nanoparticles. Journal of Membrane Science, 387-388, 40-47 (2012).

Espina, V. S., Jaffrin, M. Y., Frappart, M. and Ding, L.-H., Separation of casein micelles from whey proteins by high shear microfiltration of skim milk using rotating ceramic membranes and organic membranes in a rotating disk module. Journal of Membrane Science, 325, 872-879 (2008).

Gekas, V. and Hallström, B., Mass transfer in the membrane concentration polarization layer under turbulent cross flow: I. Critical literature review and adaptation of existing sherwood correlations to membrane operations. Journal of Membrane Science, 30, 153-170 (1987).

Ho, C.-C. and Zydney, A. L., Effect of membrane morphology on the initial rate of protein fouling during microfiltration. Journal of Membrane Science, 155, 261-275 (1999).

Ho, C.-C. and Zydney, A. L., A Combined pore blockage and cake filtration model for protein fouling during microfiltration. Journal of Colloid and Interface Science, 232, 389-399 (2000a).

Ho, C.-C. and Zydney, A. L., Measurement of membrane pore interconnectivity. Journal of Membrane Science, 170, 101-112 (2000b).

Ho, C.-C. and Zydney, A. L., Transmembrane pressure profiles during constant flux microfiltration of bovine serum albumin. Journal of Membrane Science, 209, 363-377 (2002).

Jim, K. J., Fane, A. G., Fell, C. J. D. and Joy, D. C., Fouling mechanisms of membranes during protein ultrafiltration. Journal of Membrane Science, 68, 79-91 (1992).

Joshi, R. N., Singh, K., Bhattacharya, A., Approaches to prepare TFC polyamide membranes by coating diamine during, and/or post formation of asymmetric membranes and their performances. Brazilian Journal of Chemical Engineering, 28, 457-465 (2011).

Kanani, D. M., Sun, X. and Ghosh, R., Reversible and irreversible membrane fouling during in-line microfiltration of concentrated protein solutions. Journal of Membrane Science, 315, 1-10 (2008).

Kelly, S. T. and Zydney, A. L., Protein fouling during microfiltration: Comparative behavior of different model proteins. Biotechnology and Bioengineering, 55, 91-100 (1997).

Kimura, K., Maeda, T., Yamamura, H. and Watanabe, Y., Irreversible membrane fouling in microfiltration membranes filtering coagulated surface water. Journal of Membrane Science, 320, 356-362 (2008).

Kwon, D. Y., Vigneswaran, S., Fane, A. G. and Aim, R. B., Experimental determination of critical flux in cross-flow microfiltration. Separation and Purification Technology, 19, 169-181 (2000).

Madaeni, S. S. and Mansourpanah, Y., Chemical cleaning of reverse osmosis membranes fouled by whey. Desalination, 161, 13-24 (2004).

Martín, A., Martínez, F., Calvo, J. I., Prádanos, P., Palacio, L. and Hernández, A., Protein adsorption onto an inorganic microfiltration membrane: Solute-solid interactions and surface coverage. Journal of Membrane Science, 207, 199-207 (2002).

Matthiasson, E. and Sivik, B., Concentration polarization and fouling. Desalination, 35, 59-103 (1980).

Mercier-Bonin, M., Fonade, C. and Gésan-Guiziou, G., Application of gas/liquid two-phase flows during crossflow microfiltration of skimmed milk under constant flux conditions. Chemical Engineering Science, 59, 2333-2341 (2004).

Mirzaie, A., Mohammadi, T., Effect of ultrasonic waves on flux enhancement in microfiltration of milk. Journal of Food Engineering, 108, 77-86 (2012).

Mohammadi, T., Madaeni, S. S. and Moghadam, M. K., Investigation of membrane fouling. Desalination, 153, 155-160 (2003).

Mourouzidis-Mourouzis, S. A. and Karabelas, A. J., Whey protein fouling of large pore-size ceramic microfiltration membranes at small cross-flow velocity. Journal of Membrane Science, 323, 17-27 (2008).

Pakizeh, M., Mansoori, S. A. A., Pourafshari Chenar, M., Namvar-Mahboub, M., Modification of PSf membrane nanostructure using different fabrication parameters and investigation of the CO_2 separation properties of PDMS-coated PSf composite membranes. Brazilian Journal of Chemical Engineering, 30, 345-354 (2013).

Palacio, L., Ho, C. C., Prádanos, P., Hernández, A. and Zydney, A. L., Fouling with protein mixtures in microfiltration: BSA-lysozyme and BSA-pepsin. Journal of Membrane Science, 222, 41-51 (2003).

Pollo, L. D., Duarte, T., Habert, A. C., Borges, C. P., Polymeric membranes containing silver salts for propylene/propane separation. Brazilian Journal of Chemical Engineering, 29, 307-314 (2012).

Rezaei, H., Zokaee Ashtiani, F. and Fouladitajar, A., Effect of operating conditions on fouling resistances at cross-flow microfiltration of whey by polyethersulfone. 13th National Iranian Chemical Engineering Congress (2010).

Rezaei, H., Zokaee Ashtiani, F. and Fouladitajar, A., Effects of operating parameters on fouling mechanism and membrane flux in cross-flow microfiltration of whey. Desalination, 274, 262-271 (2011).

Samuelsson, G., Dejmek, P., Trägårdh, G. and Paulsson, M., Minimizing whey protein retention in cross-flow microfiltration of skim milk. International Dairy Journal, 7, 237-242 (1997).

Saxena, A., Tripathi,. B. P., Kumar, M., Shahi, V., Membrane-based techniques for the separation and purification of proteins: An overview. Advances in Colloid and Interface Science, 145, 1-22 (2009).

Tracey, E. M. and Davis, R. H., Protein fouling of track-etched polycarbonate microfiltration membranes. Journal of Colloid and Interface Science, 167, 104-116 (1994).

Velasco, C., Ouammou, M., Calvo, J. I. and Hernández, A., Protein fouling in microfiltration: deposition mechanism as a function of pressure for different pH. Journal of Colloid and Interface Science, 266, 148-152 (2003).

Vera, L., Delgado, S. and Elmaleh, S., Dimensionless numbers for the steady-state flux of cross-flow microfiltration and ultrafiltration with gas sparging. Chemical Engineering Science, 55, 3419-3428 (2000).

Wang, F., Tarabara, V. V., Pore blocking mechanisms during early stages of membrane fouling by colloids. Journal of Colloid and Interface Science, 328, 464-469 (2008).

Wang, Z., Cui, Y., Wu, W., Ji, S., Yao, J., Zhang, H., Zhao, X., The convective model of flux prediction in a hollow-fiber module for a steady-state cross-flow microfiltration system. Desalination, 238, 192-209 (2008).

Zokaee Ashtiani, F., Kaghaghazchi, T. and Zare, A., Cell harvesting by microfiltration in a deadend system. Process Biochemistry, 34, 803-810 (1999).